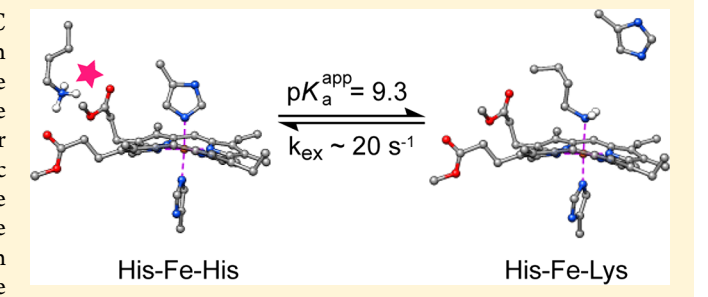
Histidine-Lysine Axial Ligand Switching in a Hemoglobin: A Role for **Heme Propionates**

Dillon B. Nye,[†] Matthew R. Preimesberger,^{†,§} Ananya Majumdar,[‡] and Juliette T. J. Lecomte*,[†]

[†]T. C. Jenkins Department of Biophysics, Johns Hopkins University, Baltimore, Maryland 21218, United States

Supporting Information

ABSTRACT: The hemoglobin of Synechococcus sp. PCC 7002, GlbN, is a monomeric group I truncated protein (TrHb1) that coordinates the heme iron with two histidine ligands at neutral pH. One of these is the distal histidine (His46), a residue that can be displaced by dioxygen and other small molecules. Here, we show with mutagenesis, electronic absorption spectroscopy, and nuclear magnetic resonance (NMR) spectroscopy that at high pH and exclusively in the ferrous state, Lys42 competes with His46 for the iron coordination site. When b heme is originally present, the population of the lysine-bound species remains too small for



detailed characterization; however, the population can be increased significantly by using dimethyl-esterified heme. Electronic absorption and NMR spectroscopies showed that the reversible ligand switching process occurs with an apparent pK, of 9.3 and a Lys-ligated population of ~60% at the basic pH limit in the modified holoprotein. The switching rate, which is slow on the chemical shift time scale, was estimated to be 20-30 s⁻¹ by NMR exchange spectroscopy. Lys42-His46 competition and attendant conformational rearrangement appeared to be related to weakened bis-histidine ligation and enhanced backbone dynamics in the ferrous protein. The pH- and redox-dependent ligand exchange process observed in GlbN illustrates the structural plasticity allowed by the TrHb1 fold and demonstrates the importance of electrostatic interactions at the heme periphery for achieving axial ligand selection. An analogy is drawn to the alkaline transition of cytochrome c, in which Lys-Met competition is detected at alkaline pH, but, in contrast to GlbN, in the ferric state only.

Teme proteins harness the heme cofactor to perform diverse chemistries using a network of interactions between the polypeptide and the prosthetic group. Among the many features that dictate reactivity, the axial ligands to the heme iron play a critical role. They are intimately involved in modulating the redox potential of the heme, the structural properties of the heme binding site, and the stability of the holoprotein.3 Most heme proteins use one or two residues to coordinate the central iron. Among the latter group, it is common for one of the ligands to undergo facile displacement, a property that adds thermodynamic, kinetic, and structural complexity to the behavior of the protein. A specific challenge in the design of functional heme proteins is not only to achieve the desired ligation scheme but also to control its stability, its lifetime, and the consequences of its disruption.⁴ The hemoglobin superfamily offers several examples of endogenous hexacoordination and can be used to explore how a common tertiary structure evolved to control axial ligand lability as demanded by distinct reactivity requirements.

"Hexacoordinate" hemoglobins use as axial ligands the conserved "proximal" histidine, located on the F helix, and a residue on the E (or distal) helix. This latter residue is most frequently a histidine (yielding a bis-histidine complex), although recently a lysine ligand has also been found in a

small number of proteins. 5-8 Endogenous hexacoordination has explicable consequences for the properties of a globin. For example, the rate of decoordination by the labile distal ligand can limit the kinetics of dioxygen binding,9 and a preserved ligand set in the ferric and ferrous oxidation states can lower the reorganization energy associated with electron transfer compared to that of systems in which the ligand set is altered. 10 In rare instances, pronounced kinetic stability of distal ligation in the ferric or ferrous state (or both) is observed. 11,12 For globin enzymes that must accomplish both small molecule binding and redox cycling, however, a balance of ligand association and dissociation rates must be reached to ensure activity on the physiological time scale.

Many studies have elucidated the properties of model hemes with axial imidazole ligands (see, for example, ref 13 and references therein). Microperoxidases, which are small proteolytic fragments of cytochrome c, have been particularly useful for describing complexes of the His-Fe-X type, ¹⁴ as has been a proximal histidine variant of myoglobin for complexes of the X-Fe-imidazole and X-Fe-amine types. ¹⁵ Nevertheless,

Received: November 14, 2017 Revised: December 21, 2017 Published: December 22, 2017

[‡]Biomolecular NMR Center, Johns Hopkins University, Baltimore, Maryland 21218, United States

controlling the properties of axial ligation has been a persistent, and formidable, objective in the de novo engineering of heme proteins. 16-19 Whereas *de novo* electron carrier proteins may be designed around a robust bis-histidine ligation scheme, the design of an asymmetric or labile coordination sphere is considerably more difficult. 4,20 Furthermore, anticipating the axial ligand set in an arbitrary protein scaffold remains a challenge. Prediction from sequence is unreliable in part because homology modeling is rarely possible at the necessary level of resolution. In addition, the static structures used to construct these models do not capture all features that may lead to ligation such as access to alternative conformational states (for example, open vs closed forms) or reduced local stability easily overcome by the formation of a coordination bond. In hemoglobins, the expectation of proximal histidine coordination is invariably satisfied, but distal ligation, let alone its thermodynamic and kinetic stability, has so far escaped prediction. Experimental data are necessary to articulate the determinants of heme coordination strength and lability.

To bind an exogenous ligand, an endogenously hexacoordinate protein must have an energetically and kinetically accessible space for the displaced axial residue. Thus, hexacoordinate globins are generally capable of a ligand-related conformational rearrangement. Structural studies illustrate that bis-histidine globins have a range of responses to exogenous ligand binding. In human cytoglobin, the distal histidine changes rotameric state and turns away from the heme when the ferrous protein binds carbon monoxide²¹ (PDB entries 2DC3 and 3AG0). In carbonmonoxy murine neuroglobin, the distal histidine retains its orientation but the heme slides deeper into the protein matrix, increasing the distance between the iron and the histidine N ϵ 2 atom²² (PDB entries 1Q1F and 1W92). Drosophila melanogaster hemoglobin undergoes a comparatively larger rearrangement involving heme sliding and displacement of a distal region (CD corner, D helix, and E helix in the canonical description of the fold) to accommodate cyanide as a ligand²³ (PDB entries 2BK9 and 2G3H). Various modes of flexibility have therefore evolved for ligand binding in these systems.

For ionizable ligands such as lysine and histidine, bonding to iron occurs in their neutral states; for a lysine side chain at physiological pH, deligation is expected to be coupled with protonation and formation of hydrogen bonds and other interactions with the solvent or the protein. Proton-coupled deligation is exemplified by the Chlamydomonas reinhardtii hemoglobin, THB1, which in the ferric state undergoes a reversible pH-dependent transition between a lysine-ligated state and a water-bound lysine-deligated state with an apparent pK₂ of $\sim 6.5.^{5}$ In another example, the well-known alkaline transition of ferric yeast iso-1-cytochrome c involves the displacement of the native Met80 ligand by Lys73²⁴ and Lys79, 25 residues otherwise exposed to solvent. The cytochrome c alkaline transition occurs with an apparent p K_a (~8.5-9.5, depending on the specific protein and sample conditions) that is higher than that in C. reinhardtii THB1. Modification of cytochromes c by mutagenesis often favors lysine ligation, suggesting that the strongly conserved protein sequence has evolved to condition its pH response.²⁶⁻²⁹ Further investigation of how hexacoordinate globins respond to changes in pH adds insights complementary to the cytochrome *c* studies.

The monomeric hemoglobin from *Synechococcus* sp. PCC 7002 (GlbN) accesses different conformations in its

endogenously hexacoordinated bis-histidine state and exogenous ligand-bound state (Figure 1).³⁰ In addition, this

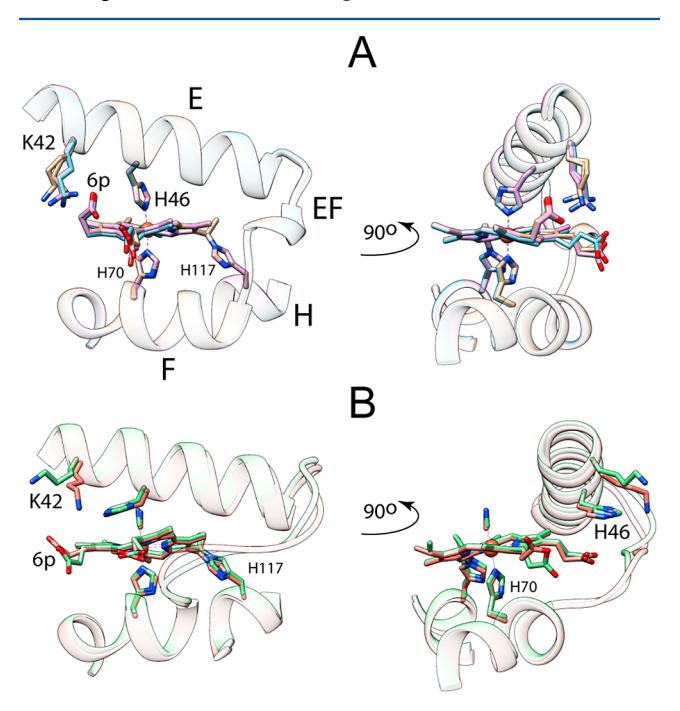


Figure 1. Heme propionate interactions in the (A) His–Fe–His and (B) His–Fe–CN structures of GlbN with PTM (GlbN-A). "6p" indicates the 6-propionate group. The E, EF, and F elements of the structure are shown as ribbons. The rest of the structure has been omitted for the sake of clarity. The asymmetric units of the crystals contain three (A, PDB entry 4MAX) and two (B, PDB entry 4L2M) monomers, which were superimposed to illustrate variability in side chain positions. The 6-propionate interacts with Lys42 in the His–Fe–His complex, whereas the 7-propionate interacts with His46 in the His–Fe–CN complex. The conformational change in the E helix and EF loop is apparent in the right panel. The heme–His117 cross-link (PTM) is shown in both structures.

cyanobacterial protein can undergo covalent attachment of the heme group, 31 a post-translational modification (PTM) that generates a c-like heme and reduces the degree of motional freedom of the heme relative to the protein matrix. The PTM mechanism is straightforward; it consists of the addition of a histidine (His117) to the α -carbon of one of the two b heme vinyl groups. The reaction occurs spontaneously in the ferrous oxidation state but not in the ferric state. 32,33 The modification has been extensively studied for its pH dependence, 33 its influence on the stability of the protein, 34 its perturbation of backbone dynamic properties, 35 and its potential utility in protein engineering. 36 The PTM yields a holoprotein that has heme attachment in common with cytochrome c, a feature that provides a bridge between two important groups of proteins. The structure of the modified heme is shown in Figure S1.

Here, we sought to probe the stability of the bis-histidine coordination scheme in GlbN and explore the conformational space accessible to the polypeptide beyond the structures depicted in Figure 1. When displaced by cyanide, the distal histidine (His46) stacks on the heme 7-propionate (Figure 1B), whereas in the bis-histidine state, a lysine (Lys42) points to the 6-propionate to form a putative salt bridge (Figure 1A). We therefore reasoned that perturbation of charge interactions at the heme periphery, as would be caused by a change in pH or heme modification, might reshape the energy surface of the

protein in a consequential way. As we will show here, an elevated pH promotes an alternative GlbN ligation scheme in a process that can be linked to the heme propionates. This observation opens new opportunities to compare and contrast ligand competition and switching in a large number of heme proteins.

MATERIALS AND METHODS

GlbN Forms under Investigation. This study required the preparation of several GlbN forms. Before PTM, the native holoprotein contains iron-protoporphyrin IX (Fe PP or b heme). We represent the ferric state of this species with Fe(III) PP GlbN. We also used the dimethyl-esterified cofactor and represent the ferric protein containing it as Fe(III) PPDME GlbN. GlbN in the ferrous oxidation state spontaneously forms a covalent linkage between Nε2 of His117 and the 2-vinyl Cα atom of the heme group (Figure S1C). For the sake of brevity, we refer to the GlbN forms with the PTM as PP GlbN-A and PPDME GlbN-A.

Protein Production and Purification. Recombinant GlbN was obtained from Escherichia coli essentially as described previously.31 Briefly, inclusion bodies of apoGlbN were solubilized in 8 M urea. The protein was refolded and purified by being passed through a Sephadex G-50 Fine (SigmaAldrich) sizing column. Fe(III) PP chloride (SigmaAldrich) was added, and the holoprotein was subjected to anion exchange chromatography on a diethylaminoethyl (DEAE) Sephacel (GE Healthcare) column. GlbN purity was confirmed using sodium dodecyl sulfate-polyacrylamide gel electrophoresis and mass spectrometry. Alternatively, no cofactor was added prior to anion exchange, and the purified apoprotein was exchanged into 1 mM potassium phosphate buffer (pH 7.0) before being stored as lyophilized powder or immediately reconstituted with Fe(III) PPDME chloride as detailed below. Uniformly ¹⁵Nlabeled GlbN was purified in the same fashion from cells grown in M9 minimal medium containing ¹⁵NH₄Cl (Cambridge Isotope Laboratories) as the sole nitrogen source. Synechocystis sp. PCC 6803 GlbN containing Fe(III) PP was prepared with a similar protocol, as described previously.³

The K42L, H46L, K48L, and H117A GlbN variants were produced using the QuikChange site-directed mutagenesis method (Qiagen, Valencia, CA) and primers purchased from IDT (Coralville, IA). The GlbN variants were purified and reconstituted with Fe(III) PP chloride³¹ prior to the anion exchange step and lyophilized for long-term storage. The K42L and H117A GlbN holoproteins were converted to the apoproteins using cold butanone (Alfa Aesar) according to the procedure described by Teale.³⁸ Following dialysis into 10 mM potassium phosphate buffer (pH 7.0), the apoprotein was reconstituted with Fe(III) PPDME chloride.

Reconstitution with Fe(III) PPDME. Fe(III) PPDME chloride (Frontier Scientific, Logan, UT) was used without further purification. Reconstitution was performed according to procedures established for iron-porphyrin derivatives with low aqueous solubility.³⁹ Fe(III) PPDME chloride was dissolved in dry dimethyl sulfoxide (DMSO, J. T. Baker) to a concentration of 5–10 mg/mL and gently added to an aqueous solution of apoGlbN [0.3–1 mM protein and 2–5 mL potassium phosphate butter (pH 7)] in a 1.1-fold molar excess. The mixture was allowed to incubate while being stirred at 4 °C, and heme binding was assessed after several hours using optical absorbance spectroscopy. Multiple additions of Fe(III) PPDME chloride to a final ~5-fold molar excess were required for

sufficient reconstitution. The final DMSO concentration was kept below 10%~(v/v), and the reaction was allowed to proceed for 12 h after the last addition. The mixture was then clarified by centrifugation, and the resulting cherry-red supernatant was applied to a DEAE anion exchange column, which precipitated any remaining free Fe(III) PPDME. The purified protein was eluted with high-salt buffer [50 mM potassium phosphate buffer (pH 7) and 100 mM NaCl] before being exchanged into 1 mM potassium phosphate buffer (pH 7.0) for lyophilization and storage. With this protocol, some apoprotein remained in the sample, which NMR spectra make apparent.

Preparation of GlbN-A. GlbN-A was prepared as reported previously. The sample of PPDME GlbN [\sim 1 mM, 50 mM potassium phosphate buffer (pH 7.1)] was reduced with \sim 5 mM dithionite (DT, SigmaAldrich) and incubated at room temperature for \sim 10 min. The sample was then oxidized with 10 mM K₃[Fe(CN)₆] and passed over a G-25 (SigmaAldrich) desalting column equilibrated in 1 mM potassium phosphate buffer (pH 7.0), concentrated using centrifugation, and lyophilized for storage. Formation of the covalent linkage between the GlbN polypeptide and PPDME was confirmed using mass spectrometry. The same procedure was applied to GlbN variants and 15 N-labeled GlbN.

pH Titration of PPDME GlbN-A by Electronic **Absorption Spectroscopy.** A concentrated sample of Fe(III) PPDME GlbN-A was diluted 50-fold into the appropriate buffer, and the electronic absorption spectrum was measured using a Cary50 ultraviolet-visible (UV-vis) spectrophotometer over the wavelength range of 800-260 nm in 1 nm steps. Ferrous ("deoxy") GlbN-A was generated by addition of 2 mM fresh DT, and spectra were collected from 750 to 350 nm every 45 s for at least 5 min after addition of DT. A series of buffers were used over a pH range of 6.4-11.3: 100 mM potassium phosphate (pH 6.4-7.8), 100 mM Tris (pH 7.8-8.8), 100 mM sodium borate (pH 8.8-9.8), 100 mM glycine (pH 9.8-10.8), and 100 mM 3-(cyclohexylamino)-1-propanesulfonic acid (CAPS) (pH 10.8-11.3). When buffers were switched, two spectra were collected at the same pH to control for the influence of the buffer. To account for small dilution errors, the ferrous GlbN-A spectra were scaled on the basis of the ferric absorbance spectra, which do not vary with pH over the studied range.

The apparent pK_a of the alkaline transition observed during the pH titration of Fe(II) PPDME GlbN-A was determined by globally fitting the Henderson—Hasselbalch equation (eq 1) to two traces (424 and 526 nm, approximate isosbestic points of a low-pH transition) using a routine implemented in Wolfram Mathematica version 10.0.2.0.

$$A_{\text{obs}}^{\lambda} = A_{\text{base}}^{\lambda} + (A_{\text{acid}}^{\lambda} - A_{\text{base}}^{\lambda}) \frac{10^{n[pK_{\text{a}}(\text{app}) - \text{pH}]}}{1 + 10^{n[pK_{\text{a}}(\text{app}) - \text{pH}]}}$$
(1)

where n is a Hill coefficient, λ is the wavelength of observation, A_{base} is the absorbance in the alkaline limit, A_{acid} is the absorbance in the acid limit, and $pK_{\text{a}}(\text{app})$ is the apparent pK_{a} of the transition.

Heme-Protein Cross-Linking Kinetics. Concentrated samples of Fe(III) PP GlbN, Fe(III) PPDME GlbN, Fe(III) PP K42L GlbN, and Fe(III) PPDME K42L GlbN were diluted into 100 mM sodium borate buffer (pH 9.2). DT (2 mM) was added to initiate the reaction, and spectra were collected from 700 to 350 nm every 45 s (or every 45 s for 10 min and then every 2 min for PPDME K42L GlbN) using a Cary50 UV-vis

spectrophotometer. The reaction of each protein was analyzed with singular-value decomposition 40 on a portion of the visible spectrum (580–540 nm). For each data set, the first two singular values are significantly larger than the third, and the first two **V** vectors were globally fit to a single exponential. In addition to PTM formation, the first **V** vector revealed a slow, low-amplitude process in the spectra that is tentatively assigned to H_2O_2 -mediated heme bleaching. Inclusion of a second exponential improved the global fit but did not affect the rate constant determined for the main process.

Acquisition and Analysis of NMR Data. NMR data were collected on either a Bruker Avance-600 or a Bruker Avance II-600 spectrometer each equipped with a TXI cryoprobe. Multidimensional data sets were processed with NMRPipe 3.0 and analyzed using Sparky3. 1D data were processed and analyzed using Topspin 3.1. 1 H chemical shifts were referenced indirectly through the (residual) water signal corrected for temperature. 15 N chemical shifts were referenced indirectly with the Ξ ratio. 41 High-pressure data were collected to a maximum pressure of 1.5 kbar using a Daedalus Innovations Xtreme-60 pump and cell apparatus equipped with a zirconia NMR cell.

NMR Sample Preparation. Fe(III) PPDME samples with and without PTM, and with and without ¹⁵N labeling, were prepared as reported previously for the wild-type protein. ³⁵ Details of sample composition and conditions are provided in the figures in the Supporting Information. Backbone, side chain, and heme assignments were obtained with a complement of homonuclear (DQF-COSY, TOCSY, and NOESY experiments) and ¹H-¹⁵N data.

Fe(II) samples were prepared under a N_2 atmosphere by first resuspending lyophilized protein in buffer that was degassed and then sparged with N_2 . The pH of the protein sample was measured prior to addition of \sim 5 mM DT to generate the ferrous state. The sample was then transferred to a Shigemi NMR tube, layered with argon, and sealed with the Shigemi plunger and Parafilm M. Samples prepared in this manner showed no indication of oxidation for weeks.

NMR Assignment of Alkaline Species. In the ferrous state at alkaline pH [1.5 mM PPDME GlbN-A, 100 mM sodium borate buffer (pH* 9.6), and 99% ²H₂O], a novel form of PPDME GlbN was observed in the ¹H 1D spectrum compared to the neutral pH spectrum [1.2 mM PPDME GlbN-A, 50 mM potassium phosphate buffer (pH* 7.1), and 99% ²H₂O]. As detailed in the Results, this new form was identified as a His-Fe-Lys complex. Simulation of selected peaks yielded the relative population of the native His-Fe-His and new His-Fe-Lys forms as a function of pH. A ¹H-¹H 2D EXSY⁴² experiment was performed at 25 °C (τ_{mix} = 30 ms) to transfer chemical shift assignments from the native conformation to this new form. The suite of ¹H-¹H 2D experiments given above was used to confirm and extend these assignments at 17 °C. The kinetics and temperature dependence of the chemical exchange allowed the cross peaks arising from exchange to be distinguished from those arising from dipolar contact in the EXSY and NOESY ($au_{
m mix}$ = 80 ms) spectra. Partial backbone ¹H-¹⁵N assignments [0.5 mM PPDME GlbN-A, 100 mM sodium borate buffer (pH 9.8), and 10% ²H₂O] were made using 2D $^{1}H-N_{z}-^{1}H$ and $^{1}H-N_{z}-^{15}N$ ZZ exchange spectra (25 $^{\circ}$ C; τ_{mix} = 50 ms) and a 3D $^{1}H-^{15}N-^{1}H$ NOESY-HSQC (17 $^{\circ}$ C; τ_{mix} = 80 ms) spectrum.^{33,43} A water presaturation ^{1}H 1D spectrum of the ferrous species was acquired at alkaline pH with a sodium carbonate/bicarbonate buffer 44 [0.5 mM PPDME GlbN-A, 90 mM sodium (bi)carbonate buffer (pH 10.5), and 10% 2 H₂O] using a 5 s recycling delay for quantification of the two forms well above the apparent p K_a of the transition (see Results).

Kinetics of Ligand Exchange. The kinetics of chemical exchange were investigated with an alkaline ferrous sample [1.5] mM PPDME GlbN-A, 90 mM sodium borate buffer (pH 9.3), and 10% ²H₂O, at 25 °C] using a modified ¹H-¹H 2D EXSY experiment that incorporated a WATERGATE solvent suppression scheme. The relaxation delay was 1.1 s, and the sorted mixing times (τ_{mix}) were 2.5, 5.0, 7.5, 10.0, 15.0, 20.0, 30.0, 50.0, 75.0, 100.0, and 150.0 ms. A two-state equilibrium represented by His–Fe–His \leftrightarrows His–Fe–Lys was assumed. The observed equilibrium constant, K_{eq} , is $\sum [His-Fe-Lys]/\sum [His-Fe-His] = k_f/k_r$, where k_f and k_r are apparent unimolecular forward and reverse rate constants, respectively. The equations governing longitudinal relaxation in the presence of chemical exchange 42 were best fit to the integrated peak intensity data to obtain the initial intensity of the resolved (His-Fe-Lys) diagonal peaks. The initial intensity of unresolved (His-Fe-His) diagonal peaks was constrained by the observed equilibrium constant, $K_{\rm eq}$. The initial slope method⁴⁵ was applied to the buildup of the exchange cross peaks. Data at the four shortest mixing times were used to avoid excessive contamination by NOEs. The initial slope, divided by the initial diagonal intensity, returns the exchange rate constant. Additional details are included in the Supporting Information.

Structural Comparison. Backbone chemical shift perturbations (CSPs) were calculated using a 15 N weighting factor of 0.1^{46} according to

$$CSP = \sqrt{0.1(\delta_{N}^{PPDME} - \delta_{N}^{PP})^{2} + (\delta_{H}^{PPDME} - \delta_{H}^{PP})^{2}}$$
 (2)

CSPs for Fe(III) PPDME GlbN used assignments published for Fe(III) PP GlbN.⁴⁷ In the case of Fe(II) PPDME GlbN-A, the CSPs were calculated between the two conformations (His–Fe–His and His–Fe–Lys) present in the same sample and identified with published assignments.^{33,47}

Multiple-Sequence Alignment. A BLAST search was performed with the sequence of GlbN as the query and expect value set to 1×10^{-6} . More than 1500 sequences were retrieved, which were filtered after Clustal alignment with the following criteria: 80% identity at most, 100 residues at least, and the presence of the proximal histidine, a pair of glycines at GlbN positions 9 and 10, and a tyrosine at position 22 (B10). The 341 qualifying sequences were then inspected for amino acid identity at GlbN positions 42 and 46.

■ RESULTS

General Features of GlbN. Synechococcus hemoglobin is a Group I truncated hemoglobin (TrHb1). It can be prepared in pure form with (GlbN-A) and without (GlbN) the His117—heme PTM. Both species merit study as they appear to be physiologically relevant in mitigating reactive nitrogen species (RNS) stress, ⁴⁸ albeit with distinct reactivities toward a common RNS, nitric oxide. ⁴⁹ Whereas it is possible to study separately GlbN and GlbN-A in the ferric state, reduction of the ferric bis-histidine form results in spontaneous PTM, ³² and therefore, only GlbN-A is readily accessible in the ferrous (deoxy) state if His117 is present. Replacement of His117 with a residue incapable of nucleophilic attack on the heme vinyl gives access to analogues of Fe(II) PP GlbN and Fe(II)

PPDME GlbN. For this purpose, the His117Ala variant was utilized.

GlbN has the typical TrHb1 fold composed of a two-on-two helical sandwich.⁵⁰ The secondary structure has seven helices, labeled A-C and E-H. Besides His117 (H helix), positions of interest in this study are His70, the proximal ligand (F helix); His46, the distal ligand (E helix); and Lys42 (E helix). The available 3D structures are the ferric bis-histidine protein (PDB entries 2KSC⁴⁸ and 4MAX³⁰) and the cyanide-bound protein (PDB entry 4L2M³⁰), all with PTM. We use the Fischer nomenclature for the heme group. IUPAC and Fischer numbering are reconciled in Figure S1. As abbreviations for iron ligation schemes, we use proximal histidine-Fe-distal ligand, e.g., His-Fe-His. Where necessary, we include the oxidation state of the iron as Fe(II) (ferrous) or Fe(III) (ferric). With regard to spectroscopic properties, His-Fe(III)-His complexes have one unpaired electron (paramagnetic, lowspin $S = \frac{1}{2}$ state), whereas the His-Fe(II)-His complexes are diamagnetic (S = 0).

Response of PP GlbN and GlbN-A to High pH. To investigate the stability of GlbN, samples were exposed to high pH and their coordination state was inspected via electronic absorption spectroscopy. Fe(III) PP GlbN and GlbN-A exhibited no change in the spectrum up to pH 10.5 (data not shown). This indicated that the affinity for hydroxide ion was too low for His46 to be displaced by a near millimolar concentration of the anion. A previous study of Fe(II) PP GlbN-A did not detect electronic absorption changes from neutral pH to pH 9.2.³³ Increasing the pH to 10.5, however, alters the spectrum noticeably (Figure S2). To identify the origin of the perturbation and in light of the heme—protein interactions depicted in Figure 1, our first approach was to replace the native cofactor with its dimethyl-esterified form (PPDME).

Effects of Propionate Esterification at Neutral pH. The purified PPDME GlbN complex was initially investigated by electronic absorption spectroscopy in the ferric oxidation state at neutral pH. Heme esterification does not affect directly the porphyrin macrocycle or vinyl groups, and major changes are not expected in the spectrum as long as the protein maintains its original low-spin bis-histidine state. Comparison to Fe(III) PP GlbN under the same experimental conditions (Figure S3) reveals an unchanged spectrum. Inspection of NMR data (Figure S4) shows resolved heme and axial histidine resonances to be minimally shifted, confirming that the His–Fe(III)—His scheme is retained.

Figure 2A illustrates a portion of the ¹H-¹⁵N HSOC spectrum of Fe(III) PP and PPDME GlbN-A. Figure 2B shows the same region for the GlbN pair. Additional GlbN cross peaks are shown in Figure S5. The majority of amide backbone assignments obtained for the His-Fe(III)-His PP complexes⁴⁷ could be transferred to the His-Fe(III)-His PPDME complexes by inspection and further verified through NOEs. Obvious chemical shift perturbations are detected for backbone amides in the proximity of the iron. Val36 shows the greatest change in ¹H shift (0.25 ppm), and Gln43 shows the greatest change in ¹⁵N shift (0.41 ppm). Because the protein is paramagnetic, shifts of this small magnitude are difficult to interpret in structural terms. They could arise directly from the displacement of a nucleus within the structure or indirectly through a perturbation of the magnetic susceptibility tensor caused by a slight alteration of heme and axial ligand geometry. Larger shifts (~1 ppm) observed for the side chains of Phe35

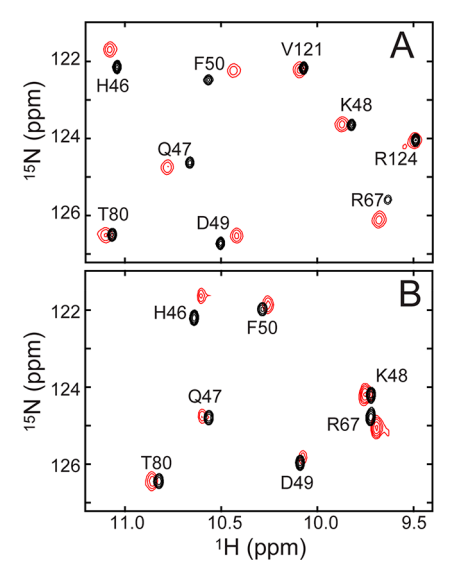


Figure 2. Portion of the ¹H–¹⁵N HSQC spectra of ferric (A) PPDME GlbN-A (red) overlaid with PP GlbN-A (black) and (B) PPDME GlbN (red) overlaid with PP GlbN (black) at neutral pH. This region of the spectrum contains hyperfine-shifted resonances. Assignments are as determined for the Fe(III) PP GlbN and GlbN-A species.⁴⁷

and Leu73, near the heme 5-CH₃, suggest local reorientation of these residues. An inspection of NOEs, however, does not indicate major changes in heme—protein or protein—protein distances. For example, one of the methylene protons of the heme 7-substituent remains in dipolar contact with Ala69 despite esterification. Overall, the data indicate a high degree of structural similarity for the Fe(III) PP and Fe(III) PPDME proteins, regardless of whether the heme—protein cross-link is present. Select chemical shifts for Fe(III) PPDME GlbN are listed in Table S1.

Turning to the ferrous state at neutral pH, we find esterification has a minor effect on the electronic absorption spectrum of Fe(II) PPDME GlbN-A compared to that of Fe(II) PP GlbN-A (Figure S3). A suite of 2D homonuclear experiments (NOESY, DQF-COSY, and TOCSY) performed at pH 7.1 was used to assign signals belonging to the heme and nearby protein side chains. Backbone assignments are available for Fe(II) PP GlbN-A,³⁵ and a comparison of the ¹H-¹⁵N HSQC spectra showed small differences caused by esterification (Figure S6). As in the ferric state, signals from the ring of Phe35 are affected and suggest a small displacement with respect to the macrocycle. We conclude that in both oxidation states and upon substitution of the heme cofactor, the protein experiences no major structural rearrangement. Nevertheless, the NMR spectral response does illustrate a propagation of the perturbation to positions remote from the propionates in the structure (e.g., Met40). Such long-range effects have also been observed in PPDME cytochrome b_5 .

PPDME GlbN-A Undergoes an Alkaline Transition in the Ferrous State. The electronic absorption spectrum of Fe(III) PPDME GlbN-A was monitored as a function of pH in the range of 6.4—11. As for Fe(III) PP GlbN-A, no change was observed (Figure S7). In the same pH range, NMR spectra supported the maintenance of stable bis-histidine ligation. We note, however, that prolonged (>1 day) incubation at pH 11 resulted in hydrolysis of the ferric heme methylesters as demonstrated by the buildup of a methanol signal at 3.33 ppm and signals attributed to singly hydrolyzed and eventually

doubly hydrolyzed (PP) heme species (not shown). The chemical instability limited NMR data collection on the Fe(III) PPDME GlbN species at high pH.

Interestingly, the minor spectral perturbations detected in Fe(II) PP GlbN-A at pH 10.5 (Figure S2) were enhanced in Fe(II) PPDME GlbN-A. Titration from pH 6.4 to 11 revealed the tail end of a low-pH process attributed to the deprotonation of the heme-linked His117 and a clear alkaline transition with onset above pH 7. The changes in the visible and Soret bands associated with this alkaline transition are line sharpening, a 1–2 nm hypsochromic shift, and a hyperchromic shift (Figure 3).

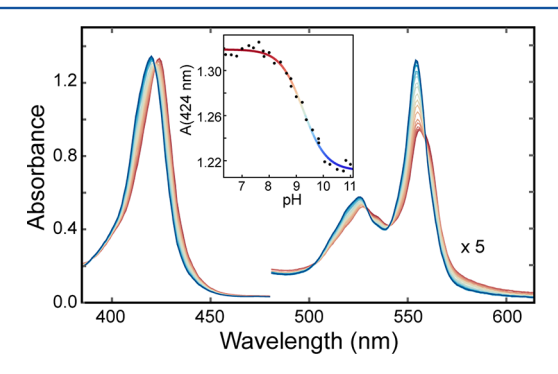


Figure 3. pH titration of Fe(II) PPDME GlbN-A. The electronic absorption spectrum is shown over the pH range from 7.4 (red) to 11 (blue). The inset presents the absorbance at 424 nm and the fit to a modified Henderson—Hasselbalch equation (apparent p K_a of ~9.3 and Hill coefficient of ~1.0).

Two wavelengths that did not respond to the low-pH process (526 and 424 nm) were chosen to characterize the alkaline transition. A modified Henderson—Hasselbalch equation was globally fitted to the data and returned an apparent pK_a of 9.26 (with error bounds of 9.20 and 9.32) and a Hill coefficient of 1.01 (0.88 and 1.15). The best-fit curve of the absorbance data at 424 nm is shown in the inset of Figure 3. Because the spectrum is insensitive to most ionization events above pH 7 [according to the behavior of Fe(III) GlbN], and the high-spin signature expected from a five-coordinate "deoxy" complex⁵² is not observed, the alkaline transition is attributed to the replacement of His46 with another strong-field ligand.

Lysine 42 Is a Ferrous Heme Distal Ligand at Alkaline **pH.** NMR spectroscopy was used to determine the identity of the supplanting axial side chain in the alkaline state. NMR data collected on Fe(II) PPDME GlbN-A at pH 7.2 and 9.7 are shown in panels A and B of Figure 4, respectively. At neutral pH, the most upfield peaks (Val121 methyl groups) resonate at approximately -1 ppm. As the pH is increased, a second set of signals appears for Val121 along with five new far upfield peaks. The shifted protons are *J*-correlated with each other, and their large negative shift must be caused by the ring current of the porphyrin macrocycle. The peak at -8.7 ppm disappears when the sample is prepared in ²H₂O and exhibits *J* coupling to a ¹⁵N nucleus resonating at approximately -37 ppm (Figure S8). These observations are consistent with axial lysine coordination as observed in C. reinhardtii THB15,53 and the M100K variant of Thiobacillus versutus cytochrome c-550.54 Thus, at alkaline pH, Fe(II) PPDME GlbN-A populates two conformations in slow exchange on the chemical shift time scale: one with native His-Fe-His ligation and the other with His-Fe-Lys ligation. ¹H NMR data collected on Fe(II) PP GlbN-A at pH 11 reveal a weak but analogous set of upfield peaks (Figure 4C),

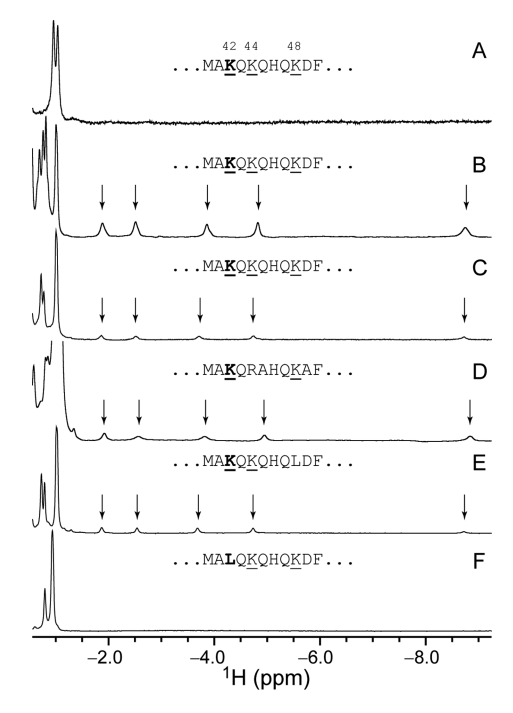


Figure 4. Upfield region of the ^1H NMR spectrum of ferrous GlbN-A: (A) PPDME GlbN-A at pH 7.2 and 25 °C, (B) PPDME GlbN-A at pH 9.7 and 25 °C, (C) PP GlbN-A at pH 10.9 and 25 °C, (D) Synechocystis PP GlbN-A at pH 11.0 and 17 °C, (E) PP K48L GlbN-A at pH 11.0 and 25 °C, and (F) PP K42L GlbN-A at pH 10.9 and 25 °C. Data collected in $^1\text{H}_2\text{O}$ with 5–10% $^2\text{H}_2\text{O}$; alkaline samples were buffered with sodium borate (B) or sodium (bi)carbonate (C–F). Vertical scaling is arbitrary; however, the population of the His–Fe–Lys form in panel B is larger than that in panel C. The Met40–Phe50 sequence is shown for each protein.

confirming that the changes detected by electronic absorption (Figure S2 and Figure 3) and NMR have the same origin regardless of whether the heme propionates are esterified.

The primary structure of GlbN contains six lysines. If the heme plane is used to divide the protein into two parts, all lysines are located in the distal part (Figure S9). Three of the six lysines are found on the A and B helices, far from the heme cofactor and presumably out of contention for iron coordination barring global unfolding. The other three, Lys42, Lys44, and Lys48, are located on the E helix. In the X-ray structure of His-Fe-His GlbN-A, Lys44 and Lys48 point away from the iron whereas Lys42 stands out as the most likely candidate, with its N ζ atom near the heme 6-propionate carboxyl group (Figure 1A). To test whether Lys42 may be an axial ligand to the iron, data were acquired on Fe(II) PP K42L GlbN-A at pH 10.9. This complex showed no evidence of lysine coordination as determined by ¹H NMR spectroscopy (Figure 4F) or electronic absorption spectroscopy (not shown). Likewise, no lysine coordination is detected in the ¹H NMR spectrum or the electronic absorption spectrum of Fe(II) PPDME K42L GlbN-A at pH 9.2 (Figure S10).

Additional support for the ligation of Lys42 is provided by the related globin from *Synechocystis* sp. PCC 6803. This protein, which is 59% identical with GlbN, has lysines at positions 42 and 48, but not at position 44. We found that *Synechocystis* GlbN-A is also capable of forming a His-Fe-Lys complex in the ferrous state under alkaline conditions (Figure 4D). Finally, we prepared the K48L variant of *Synechococcus* GlbN in the ferrous GlbN-A state at high pH, and it too

presents the signature signals of coordinated lysine (Figure 4E). Thus, Lys42 is a plausible heme ligand in Fe(II) PP GlbN-A and Fe(II) PPDME GlbN-A at high pH and is assigned as such. Propionate esterification favors the population of the His–Fe–Lys species and allows for more extensive characterization than possible with the natural cofactor.

Thermodynamics of Lysine Ligation. From the electronic absorption data, the apparent pK_a for the alkaline transition of Fe(II) PPDME GlbN-A is ~9.3 (Figure 3), but because the absorption coefficient of the His-Fe-Lys form of Fe(II) PPDME GlbN-A is not known, the limiting fractional population of the alkaline form is also unknown. An estimate can be made from integration of NMR data collected at pH 10.5: an appreciable amount of the His-Fe-His species is present, accounting for ~45% of the sample (Figure S11). This measurement was performed within 45 min of exposure of the PPDME protein to high pH and is consistent with NMR data collected at different pH values. The titration end points are therefore the His-Fe-His state, in which Lys42 is "out" and protonated, on the acidic side, and a nearly equal mixture of His-Fe-His and His-Fe-Lys states, in which Lys42 and His46 are neutral, on the alkaline side.

A simple equilibrium model capturing the pH response of Fe(II) PPDME GlbN-A is presented in Figure 5, where the

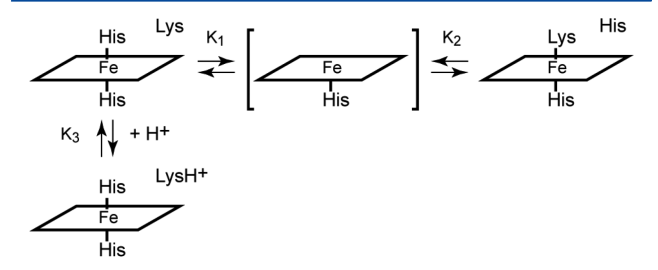


Figure 5. Proposed equilibria involving heme axial ligands in the ferrous state. K_1 and K_2 are decoordination constants. K_3 is the lysine acid dissociation constant in the bis-histidine state. The five-coordinate species (bracketed) is included for generality as many hexacoordinate globins have weak distal ligand affinity.

five-coordinate species is included but negligibly populated by GlbN under all conditions. The histidine-lysine competition is assigned an equilibrium constant $K_{\rm eq}$ = [His–Fe–Lys]/[His–Fe–His] = K_1/K_2 , where K_1 and K_2 are the decoordination constants for distal histidine and lysine, respectively. K_3 is the acid dissociation constant of the lysine when it is not ligated to the iron. The ionization equilibrium for the axial histidine is unnecessary to consider in this pH range. With these constants, the populations of the main species can be calculated and related to the spectroscopic observables (sum of His-Fe-His species and sum of His-Fe-Lys species). The apparent equilibrium for ligand switching is then expressed as K_{app} = $10^{-9.3} = (1 + K_1/K_2)K_3$ (derivation in the Supporting Information). The NMR population estimate at high pH suggests that $K_{\rm eq} = K_1/K_2 \sim 1.4$. Thus, p K_3 is constrained to be 9.7, only \sim 0.4 unit above the apparent pK of 9.3 and \sim 0.7 pH unit lower than the expected pK_a of 10.4 for an unperturbed lysine. Additional information will be needed to understand the origin of a shift in the pK_a of the decoordinated lysine (e.g., specific interactions) or to consider a "trigger group", the ionization of which is coupled to ligand switching.⁵⁵ Regardless of the mechanistic details, the model allows for a prediction of His-Fe-His and His-Fe-Lys populations at arbitrary pH values (Figure 6).

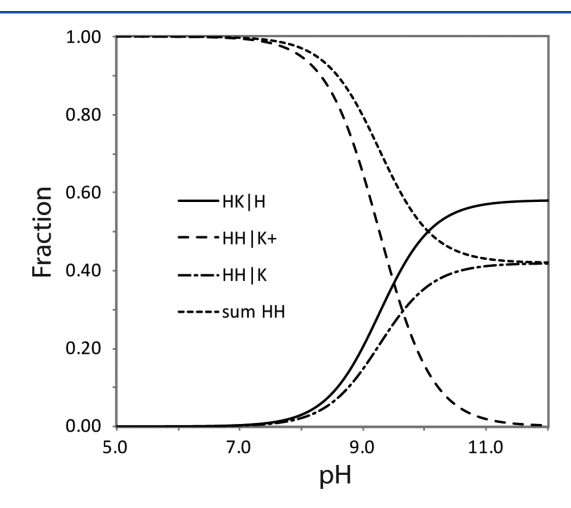


Figure 6. Population plot obtained with the scheme depicted in Figure 5. The apparent pK of the alkaline transition is 9.26, and the fraction of protein with a distal lysine ligand (HKlH) is 0.55 at pH 10.5. The value of p K_3 is then 9.64. K_1/K_2 is 1.38, corresponding to a free energy difference of 0.8 kJ mol⁻¹ favoring the lysine-bound form.

Response of the Alkaline Form to Pressure. The structural change necessary to coordinate Lys42 is expected to result in a change in volume. In an attempt to increase the population of the His–Fe–Lys conformation for NMR characterization, a sample of Fe(II) PPDME GlbN-A at pH ~9.5 was subjected to an increase in hydrostatic pressure. The ¹H NMR data presented in Figure S12 show the disappearance of the His–Fe–Lys species and an increase in the population of the His–Fe–His species as the pressure is increased to 1.5 kbar. The pH drift accompanying the compression of the borate buffer is significant ⁵⁶ but does not account fully for the shift in equilibrium. This result eliminates the use of pressure to promote lysine coordination but shows that the system adopts a greater volume when in the lysine-ligated conformation than when in the histidine-ligated conformation.

Rate of Ligand Switching and NMR Assignments at Alkaline pH. Further homonuclear experiments exploited the slow exchange between the His–Fe–Lys and His–Fe–His complexes. Correlations detected for the axial Lys in $^1\text{H}-^1\text{H}$ EXSY data place the $\text{C}\delta\text{H}_2$ and $\text{C}\epsilon\text{H}_2$ signals of Lys42 at 1.7 and 3.1 ppm, respectively, in the His–Fe–His state (Figure 7) and, as expected from the bis-histidine crystal structure, are in agreement with exposure to solvent. The intensity of the exchange cross peaks was measured as a function of mixing time (Figure S13) and treated with an initial slope approach. Combined with the equilibrium information from the pH titration, the data provide an estimate for the apparent rate constants describing the conversion of His–Fe–His to His–Fe–Lys coordination as $k_{\rm f} \sim 8~{\rm s}^{-1}$ and the reverse process as $k_{\rm r} \sim 15~{\rm s}^{-1}$ at pH 9.3 and 25 °C.

The same $^1H-^1H$ EXSY data show that the imidazole $C\delta 2H$ and $C\varepsilon 1H$ signals of His46 move from 0.5 and 1.6 ppm in the His–Fe–His conformation to 7.6 and 8.1 ppm, respectively, in the His–Fe–Lys conformation. Thus, when Lys42 is not coordinated, its two terminal methylenes ($C\delta H_2$ and $C\varepsilon H_2$) exhibit shifts that agree with exposure to solvent, whereas the ring protons of decoordinated His46 deviate from the expected

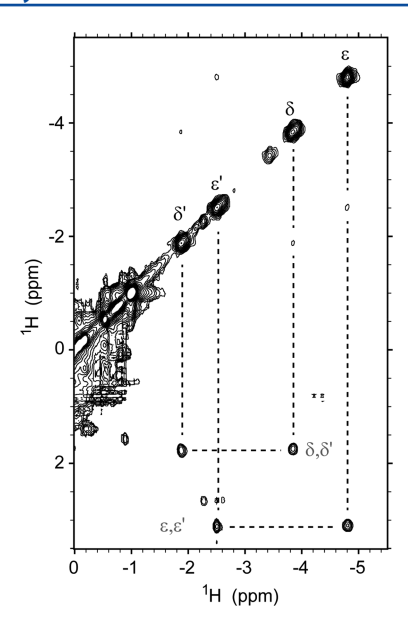


Figure 7. Portion of the $^{1}\text{H}-^{1}\text{H}$ EXSY spectrum collected on Fe(II) PPDME GlbN-A at pH 9.3 with a mixing time of 5 ms. The upfield peaks arising from the coordinated Lys42 C δ H₂ and C ϵ H₂ protons have exchange cross peaks with their decoordinated counterparts at 1.7 and 3.1 ppm.

random coil values of \sim 7 and \sim 7.7 ppm for a neutral histidine.⁵⁷ This suggests that in the alkaline conformation, His46 remains in contact with the heme or protein residues.

If the neutral-pH structures serve as guides, ligation of Lys42 requires considerable distortion of the E helix upstream of His46. This was investigated with additional NMR data at pH values within the alkaline transition. As mentioned above, 2D $^{1}H-^{1}H$ EXSY experiments performed at 25 °C connect the signals of Lys42 in the two species. The same experiment complemented with the standard suite of homonuclear data allowed the transfer of heme and additional side chain assignments to the alkaline form. Data were also collected at pH 9.6 and 17 °C in an attempt to alleviate some of the overlap. To illustrate the quality of the data at this temperature, an annotated portion of the DQF-COSY spectrum is shown in Figure S14. The heme and select side chain chemical shifts of both conformations of Fe(II) PPDME GlbN-A are listed in Table S2.

Amide assignments were obtained with 2D ¹H-N₂-¹⁵N ZZ exchange data (Figure S15), 2D ¹H-N_z-¹H ZZ exchange data [25 °C and pH 9.2 (Figure S16A)], and 3D ¹H-¹⁵N-¹H NOESY-HSQC data (17 °C and pH 9.2). Overall, the amide shifts of the His-Fe-His conformation of Fe(II) PPDME GlbN-A at pH 9.2 and PP GlbN-A at pH 7.1 are similar. In contrast, the His-Fe-Lys conformation of Fe(II) PPDME GlbN-A gives rise to a distinct ¹H-¹⁵N correlation map. The annotated 2D ¹H-N_z-¹H ZZ exchange spectrum shown in Figure S16A identifies 32 resolved correlations between amide resonances in the His-Fe-His and His-Fe-Lys forms. Some amides, such as that of Lys42, were assigned only in the His-Fe-His conformation and showed strong magnetization transfer to the water frequency. The alkaline pH necessary to populate the His-Fe-Lys form permitted only partial ¹H-¹⁵N assignments. Solvent exchange also confounded the measurement of conformational exchange rates using ¹H-N_z-¹⁵N ZZ data. However, the chemical shift separations detected between the two conformations in the ${}^{1}H-N_{z}-{}^{15}N$ ZZ and ${}^{1}H-N_{z}-{}^{1}H$

ZZ spectra are consistent with the apparent rate constants determined for the lysine side chain with EXSY data. The His—Fe–Lys resonances observed by ¹H–¹⁵N HSQC respond to pH (not shown) and pressure (Figure S13) in concert with the upfield Lys42 peaks, supporting a global rather than local conformational change upon ligand switching.

Structural Consequences of Lys42 Ligation. A coarse picture of the structural properties of the His-Fe-Lys conformation of Fe(II) PPDME GlbN-A can be gleaned from the NMR data by comparison to the His-Fe-His conformation. In Figure 8, backbone amide CSPs are colored

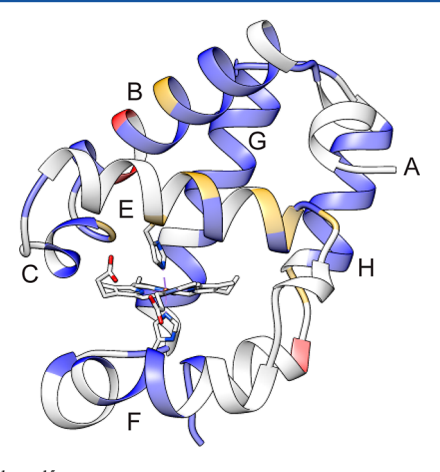


Figure 8. $^{1}H^{-15}N$ backbone CSPs obtained by comparison of the His–Fe–His and His–Fe–Lys forms of Fe(II) PPDME GlbN-A (pH 9.8) depicted on the His–Fe–His structure (PDB entry 4MAX): blue (CSP < 0.95 ppm), gold (0.95 ppm < CSP < 1.40 ppm), and red (1.40 ppm < CSP). The average CSP is 0.50 ppm, and the standard deviation is 0.45 (Figure S16). Backbone amides colored gray could not be assigned at this alkaline pH.

on the His-Fe-His GlbN-A structure according to their magnitude (values are shown in Figure S16B). The subset of amides detectable at alkaline pH forms a pattern by which the F-H helices are relatively unperturbed. The largest changes in amide chemical shift are observed for the B, C, and E helices. In addition, many resonances from the heme and several side chains on both sides of the heme experience measurable shifts [>0.2 ppm (Table S2)]. The proximal histidine and adjacent residues are among those affected. These data, although distorted by the large and anisotropic effect of the porphyrin ring current, demonstrate a structural rearrangement of the heme cavity.

Additional features of the His-Fe-Lys conformation were derived from the ¹H-¹H NOESY data. A series of characteristic dipolar contacts are recognized in both His-Fe-His and His-Fe-Lys states. These stem from the proximity of Thr80 and His83 (forming a resilient hydrogen-bonded cap),⁵⁸ interactions between Val121 and His70, contacts between Phe84 and His117, and packing of Phe61 against the heme 8-CH₃. When Lys42 or His46 acts as a heme ligand, each exhibits dipolar contact with Phe35, and common heme-protein contacts are observed for Phe35 in both conformations. Of note are the effects observed among Phe50, the heme group, and either His46 (His-Fe-His state) or the axial lysine (His-Fe-Lys state) (Figure 9). When His46 is ligated to the iron, the imidazole C ε 1H is oriented toward Phe50 on the α -meso side of the heme; in this conformation, the distance between Phe50 and Lys42 side chains is ~14 Å (Figure 9A). Figure 9C

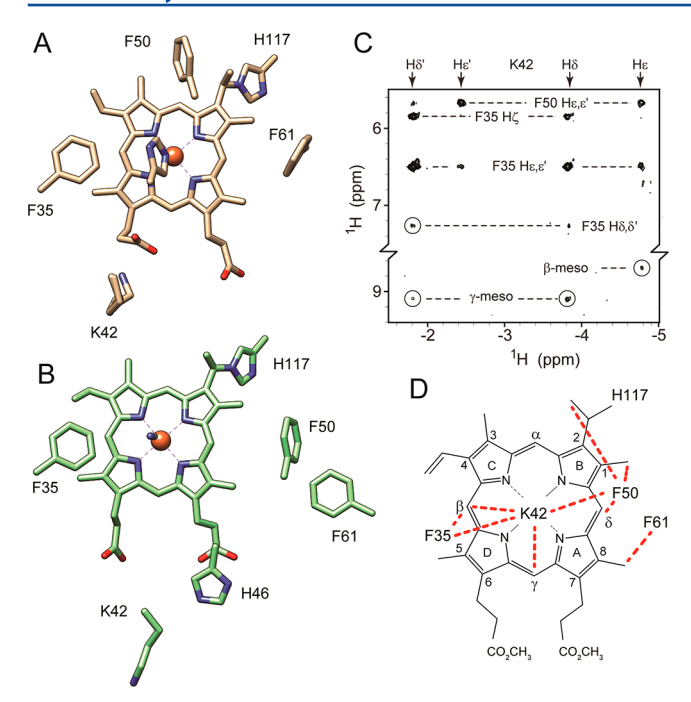


Figure 9. Structural changes in Fe(II) PPDME GlbN-A associated with axial lysine ligation. Key residues are shown in the (A) His–Fe—His and (B) His–Fe–CN X-ray structures. (C) Portion of a NOESY spectrum (pH* 9.6, 99% 2 H₂O, 17 $^\circ$ C, 80 ms mixing time) illustrating Lys42 cross peaks in the His–Fe–Lys conformation. (D) The network of observed NOEs (red dashed lines) does not correspond to either known structure (A and B) and requires a reorganization of the E helix.

presents a portion of the ¹H-¹H NOESY map showing contacts made by the $C\delta H_2$ and $C\varepsilon H_2$ protons of coordinated Lys42 with Phe50 in addition to Phe35 and the heme meso protons. In the alkaline conformation, Phe50 apparently moves "below" pyrrole B as the E helix reorients, making new contacts with the heme and the axial lysine. Analogous to the environment surrounding the Lys53 distal ligand in C. reinhardtii THB1,6,53 the proximity of coordinated Lys42 with Phe50 and Phe35, along with the presence of Phe21 and Tyr22 on the B helix, may produce a relatively hydrophobic heme distal pocket in which the lysine $N\zeta H_2$ group is protected from rapid exchange with solvent and can be observed by NMR spectroscopy. Interestingly, the constellation of NOEs detected in the His-Fe-Lys conformation (Figure 9D) differs from that expected of both the His-Fe-His (Figure 9A) and His-Fe-CN (Figure 9B) states, illustrating the plasticity of the GlbN heme pocket.

Lys42 Ligation and PTM. The conformational changes required for lysine ligation in Fe(II) GlbN-A raise two questions. First, is heme–protein cross-linking necessary to stabilize the His–Fe–Lys state, and second, does the nonnative conformation influence the rate of the PTM? NMR signals characteristic of bound lysine are detected in Fe(II) PPDME H117A GlbN and in freshly reduced, high-pH Fe(II) PPDME GlbN samples, prior to PTM (data not shown). We conclude that covalent attachment of the heme to the protein is not required for the alternative ligation state.

At pH 9.2, formation of the His117—heme covalent linkage, which requires protonation of the vinyl group, is sufficiently slow $[(2.3 \pm 0.1) \times 10^{-3} \text{ s}^{-1}]$ that the reaction can be observed optically by manual mixing of the unmodified ferric protein

with DT.³³ The His-Fe-His/His-Fe-Lys ligand exchange occurs much faster (~20 s⁻¹) and essentially establishes a condition of rapid pre-equilibrium. The ability of Fe(II) PPDME GlbN to undergo the PTM was inspected by manual mixing at pH 9.2 (Figures S17 and S18). A 2-fold reduction in the apparent rate constant for PTM formation is observed [(1.0 $\pm 0.1) \times 10^{-3}$ s⁻¹], which suggests that ligand exchange retards the reaction. Control experiments performed with PPDME K42L GlbN and PP K42L GlbN return rate constants of (1.7 \pm $0.1) \times 10^{-3}$ and $(2.7 \pm 0.1) \times 10^{-3}$ s⁻¹, respectively, both close to the wild-type value. Only the protein exhibiting ligand exchange has a clearly decelerated rate constant, by a factor approximately consistent with the pre-equilibrium factor. This may be linked to the conformational difference between the two ligation schemes. However, the effect is small, and the variations observed in the control experiments highlight the sensitivity of the rate constant to multiple factors.

DISCUSSION

Composition of Alkaline Samples and Limitations to Their Characterization. The high-pH conditions required to populate the His—Fe—Lys complex impose severe restrictions on the extent of structural and kinetic analyses that can be performed. Backbone amide exchange rates are accelerated, and many useful NMR spectroscopic handles are therefore obliterated. Furthermore, in PPDME GlbN samples, hydrolysis of the heme dimethyl esters occurs over the course of NMR data acquisition. Although the hydrolysis rate is slower in the ferrous state than in the ferric state and allows for the collection of multidimensional data sets, the complexity borne out by the presence of multiple exchanging species in evolving amounts and the limited number of spectral probes prevented a detailed description of the His—Fe—Lys complex. With these limitations in mind, we derive the following points.

Lysine versus Histidine as an Axial Ligand. The competition between the two nitrogenous ligands for axial ligation on the distal side requires an explanation. In particular, Lys42 appears to be capable of displacing His46 as the distal ligand in the ferrous (Figures 3 and 4) but not the ferric (Figure S7) oxidation state of the heme iron. The strength of an iron-ligand coordination bond opposed to a histidine axial ligand is difficult to measure experimentally in part because the pentacoordinate state of Figure 5 is often inaccessible.⁵⁹ However, studies of equilibrium binding of nitrogenous ligands to ferric heme peptide N-acetylmicroperoxidase-8 found that imidazole and propylamine were equally apt at displacing bound water. 60 If this observation is taken to be applicable to Fe(III) GlbN, the sole persistence of His-Fe-His coordination at alkaline pH may then represent entatic control⁶¹ exerted by the protein scaffold in maintaining the native ligand set.

Theoretical calculations estimate that the heme Fe(III)—imidazole Fe–N bond is $\sim\!30$ kJ/mol stronger than the Fe(II)—imidazole Fe–N bond. 59 In addition, studies of sequential histidine ligation in His–Fe–His model peptides have demonstrated that the second histidine binds ferrous iron with an affinity lower than that of the first, whereas the opposite is true in the ferric oxidation state. 62 Displacement of the iron from the porphyrin plane and steric occlusion by the pyrrole nitrogens destabilizes ferrous bis-histidine ligation. This "face strain" was invoked in discussing the heightened flexibility of ferrous GlbN as pictured by 15 N relaxation data. 35 The weaker histidine ligation and increased flexibility of GlbN-A in the ferrous state likely contribute to the ability of Lys42 to displace

His46 as the distal iron ligand. Dedicated studies will be needed to reconcile the results of different model systems and clarify the energetics of histidine and lysine ligand exchange in both iron oxidation states.

Effect of Propionate Esterification. At alkaline pH (>8), the heme propionate groups are expected to be deprotonated and negatively charged.⁶³ The structure of the His-Fe-His conformation (Figure 1) suggests that an electrostatic interaction exists between the charged Lys42 and the 6propionate. In the Fe(II) PP GlbN-A complex, the His-Fe-His conformation is fully populated at pH 9.233 and the His-Fe-Lys conformation is present as only a minor form at pH 11 [~20% (Figure 4C)]. This result indicates that strongly basic conditions are required to disrupt the Lys42-heme 6propionate interaction. Upon propionate esterification, however, the His-Fe-Lys form is populated to a significant degree at pH 9 (~20%) and reaches a maximum of ~60% at pH 11 (Figure 6). The heme modification must therefore lower the pK_a of some ionizable group, the most likely candidate being Lys42. It appears that the interaction between the 6-propionate and Lys42 prevents this residue from displacing His46 at pH ≤10 and contributes to the stability of the His-Fe-His complex. This is in contrast to the proposed role of the heme propionates in the alkaline transition of ferric cytochrome *c*, deprotonation of which may promote lysine coordination. ^{64–66} In this protein, the heme propionates are not exposed to solvent and do not interact strongly with lysines, which contributes to the distinct behavior.

Structural Perturbation and Flexibility of the E Helix. The CSP and NOE results lead to limited conclusions about the conformational rearrangement required for lysine ligation. Much of the protein undergoes some perturbation, including many of the residues composing the heme binding pocket. Not surprisingly, the largest manifestations are detected on the distal side and in particular the E helix (Figure 8). The observed contacts between Lys42 and Phe50 in the His–Fe–Lys conformation appear to require some change in secondary structure (Figure 9). One model consistent with the data involves loss of helical content for at minimum the first five residues (40–44).

The plausibility of a local structural distortion can be assessed with known properties of GlbN. At neutral pH, the backbone amides composing the N-terminal portion of the E helix of Fe(III) PP GlbN (residues 40–46) have low protection factors, becoming undetectable within a few minutes after dissolution of the protein into ²H₂O.³⁴ The modest local stability for this region of the protein is consistent with ¹⁵N relaxation measurements, 35 which show an increased level of millisecond motions on the distal side of Fe(II) PP GlbN-A relative to the rest of the protein. This is enhanced for the carbon monoxy adduct of Fe(II) PP GlbN-A, in which the first turn of the E helix has elevated R2 values. Heightened flexibility in the ferrous, compared to ferric, GlbN-A extends throughout the protein backbone whether in the bis-histidine state or with an exogenous ligand bound. In amide HSQC spectra of Fe(II) PPDME GlbN-A acquired at basic pH, we were unable to detect most of the signals arising from the N-terminal region of the E helix, likely because of rapid hydrogen exchange. These observations agree with the notion that residues 40-44 are prone to unfolding.

Lysine as a Heme Ligand and Ligand Switching. Coordination of a lysine residue requires a neutral amino group, that is, an energetic expenditure to lower the pK_a of that

group to the physiological range. In GlbN, the His-Fe-Lys state is significantly populated at pH values much higher than neutral, which suggests that per se the alternative ligation mode is unlikely to have functional significance. Likewise, the artificial PPDME prosthetic group used to populate the His-Fe-Lys conformation has no direct biological relevance. However, both high pH and propionate esterification reveal an energetically low-lying conformation that GlbN and relatives can sample and perhaps adopt when interacting with a binding partner.

It is interesting to note that, in approximately 51% of TrHb1s, a histidine occupies the same position as His46 (termed E10 by sequence analogy to the myoglobin notation, but topologically equivalent to E7 in that protein). Whether this residue is an axial ligand in all instances of TrHb1 is uncertain. It is likely that coordination occurs with different stability and population of the five-coordinate intermediate shown in Figure 5.67 Approximately 30% of TrHb1s have a lysine at the analogous position as Lys42 (E6), and 35% of those having a histidine at E10 have lysine at E6 (additional statistics are listed in Table S3). Synechocystis GlbN illustrates a second example of His/Lys ligand swapping (Figure 4D). Given the statistics, we expect that switching occurs in many TrHb1s, with a range of apparent p K_a values. In a survey of bheme proteins regardless of the fold, lysine is found to interact with a heme propionate in only 10% of tabulated instances. Arginine, in contrast, is present in 38% of the instances.⁶⁸ The enrichment of lysine at the edge of the heme cavity in GlbN relatives may signify a specific functional requirement related to iron coordination.

The structure of murine neuroglobin, a bis-histidine globin of the same lineage as myoglobin, shows an interaction between Lys67 (E10, three residues beyond the distal His E7) and a heme propionate group that is disrupted upon CO binding. When the distal histidine is replaced with a leucine residue, Lys67 is able to coordinate the ferrous heme with an apparent pK_a of 10. Similarly, a bis-histidine Arabidopsis hemoglobin has recently been shown to use Lys69 (E10) as a ferrous heme ligand when the distal histidine (His66, E7) is replaced. In contrast, the H46L variant of GlbN-A appears predominantly pentacoordinate in the ferrous state even at alkaline pH (Figure S19). As no lysine coordination is detected, these results probably reflect the effect of a leucine at the distal position, either favoring the pentacoordinate state or interfering with a potential His-Fe-Lys conformation.

An Intriguing Parallel to Cytochrome c. Distal ligand replacement has gained considerable attention over the years for its importance in sensing and signaling. ^{71,72} Various triggers have been identified, for example, a redox state change in the *E. coli* direct oxygen sensor (EcDos), ⁷³ binding of CO to the transcription factor CooA, ⁷⁴ and changes in pressure in cytochromes P420 and P450. ⁷⁵ A timely example of pH-triggered ligand switching is provided by cytochrome *c*, in which structural changes related to deligation of the axial Met80 allow the cytochrome to transform itself from an electron carrier to a peroxidase and act as an early signal in apoptosis. ^{76–79} There is now some evidence that His–Fe–Lys conformers detected through alkaline transitions contribute to the complex relationship between structure and function in the cytochrome. ^{80,81}

The response to pH exhibited by Fe(II) PPDME GlbN-A is reminiscent of the Fe(III) cytochrome Met-to-Lys switch, but with some differences. The cytochrome transition involves replacement of the axial Met80, a ligand that is "softer" than

His46 in GlbN. Lys73 and Lys79, however, are unable to displace Met80 in the ferrous oxidation state⁸² despite the relatively weak Fe-Met bond.⁵⁹ This implies a significantly reduced stability of lysine ligation in the ferrous state, consistent with the low reduction potential of the alkaline form. 82 The K73H variant undergoes a His-Fe-His to His-Fe-Lys transition in the ferric state, 83 whereas GlbN-A does not seem to depart from the His-Fe-His state when oxidized, highlighting the role of the protein scaffold in ligand selection. As an additional common feature, both GlbN-A and yeast iso-1cytochrome c exhibit heightened backbone motions on the microsecond to millisecond time scale in the oxidation state capable of ligand switching. 35,84,85 Residual dipolar coupling and ¹H-¹⁵N NOE measurements on alkaline K79A cytochrome c are consistent with increased picosecond to nanosecond motions in the ferric His-Fe-Lys form relative to the His-Fe-Met form. 86 However, human cytochrome c displays greater rigidity in the ferric oxidation state^{87,88} while still undergoing the alkaline transition, albeit with a pK_a higher than that of the yeast protein.⁸⁹ Thus, the connection between local and global backbone dynamics and ligand switching, which occurs on the millisecond to second time scale, remains to be established. The full consequences of lysine ligation in GlbN-A are unknown, but it is clear that such a scheme is made possible by the low local stability of several structural elements and imparts a different conformation beyond the edge of the heme cavity. The inability of the ferric state to undergo the same distal ligand transition as the ferrous state raises an interesting avenue to a redox sensing mechanism.

CONCLUSION

The heme propionates have been implicated in adjusting multiple holoprotein properties. $^{90-94}$ In this study, we have shown that electrostatic interactions along the heme periphery play a part in determining the coordination state of the cyanobacterial TrHb1, GlbN. For residues such as lysine, which can both form salt bridges and act as potential heme ligands, interaction with the propionates may effectively compete with iron coordination. Perhaps more importantly, we characterized a ligand switching process occurring on the subsecond time scale in one of two common oxidation states and leading to a stable conformation not captured in the existing structural models. These results exemplify well the malleability of the GlbN heme distal pocket and expand our view of the conformational landscape available to TrHb1s. Studies of other proteins with similar lysine-heme interactions are in progress to explore the generality of this mode of electrostatic control.

ASSOCIATED CONTENT

S Supporting Information

The Supporting Information is available free of charge on the ACS Publications website at DOI: 10.1021/acs.bio-chem.7b01155.

Figures S1–S19, Tables S1–S3, and the derivation of the apparent pK_a equation (PDF)

AUTHOR INFORMATION

Corresponding Author

*E-mail: lecomte jtj@jhu.edu. Telephone: (410) 516-7019.

ORCID ®

Juliette T. J. Lecomte: 0000-0003-1116-0053

Present Address

§M.R.P.: Cellmig Biolabs Inc., Cambridge, MA 02142.

Funding

This work was supported by National Science Foundation Grant MCB-1330488 to J.T.J.L. and National Institutes of Health Grant T32 GM080189 (D.B.N.).

Notes

The authors declare no competing financial interest.

ACKNOWLEDGMENTS

The authors thank Belinda Wenke, Emily Adney, and Lukas Gilevicius for preparation of *Synechocystis* GlbN, K42L GlbN, and wild-type GlbN.

ABBREVIATIONS

1D, one-dimensional; 2D, two-dimensional; 3D, three-dimensional; CSP, chemical shift perturbation; DEAE, diethylaminoethyl; DMSO, dimethyl sulfoxide; DT, sodium dithionite; EXSY, exchange spectroscopy; Fe PP, iron-protoporphyrin IX; Fe PPDME, iron-protoporphyrin IX dimethylester; GlbN, *Synechococcus* sp. PCC 7002 hemoglobin; GlbN-A, GlbN with a His117—heme covalent attachment; Hb, hemoglobin; HSQC, heteronuclear single-quantum coherence; NOE, nuclear Overhauser effect; PDB, Protein Data Bank; pH*, pH uncorrected for the isotope effect; PTM, post-translational modification; RNS, reactive nitrogen species; THB1, hemoglobin 1 from *C. reinhardtii*; TrHb1, Group I truncated hemoglobin.

REFERENCES

- (1) Kepp, K. P. (2017) Heme: From quantum spin crossover to oxygen manager of life. Coord. Chem. Rev. 344, 363-374.
- (2) Rydberg, P., Sigfridsson, E., and Ryde, U. (2004) On the role of the axial ligand in heme proteins: a theoretical study. *JBIC, J. Biol. Inorg. Chem.* 9, 203–223.
- (3) Gibney, B. R. (2016) Equilibrium studies of designed metalloproteins. *Methods Enzymol.* 580, 417–438.
- (4) Koder, R. L., Anderson, J. L. R., Solomon, L. A., Reddy, K. S., Moser, C. C., and Dutton, P. L. (2009) Design and engineering of an O₂ transport protein. *Nature* 458, 305–U64.
- (5) Johnson, E. A., Rice, S. L., Preimesberger, M. R., Nye, D. B., Gilevicius, L., Wenke, B. B., Brown, J. M., Witman, G. B., and Lecomte, J. T. J. (2014) Characterization of THB1, a *Chlamydomonas reinhardtii* truncated hemoglobin: linkage to nitrogen metabolism and identification of lysine as the distal heme ligand. *Biochemistry* 53, 4573–4580
- (6) Rice, S. L., Boucher, L. E., Schlessman, J. L., Preimesberger, M. R., Bosch, J., and Lecomte, J. T. J. (2015) Structure of *Chlamydomonas reinhardtii* THB1, a group 1 truncated hemoglobin with a rare histidine-lysine heme ligation. *Acta Crystallogr., Sect. F: Struct. Biol. Commun.* 71, 718–725.
- (7) Teh, A. H., Saito, J. A., Najimudin, N., and Alam, M. (2015) Open and Lys-His hexacoordinated closed structures of a globin with swapped proximal and distal sites. *Sci. Rep. 5*, 11407.
- (8) Ilcu, L., Rother, W., Birke, J., Brausemann, A., Einsle, O., and Jendrossek, D. (2017) Structural and functional analysis of latex clearing protein (Lcp) provides insight into the enzymatic cleavage of rubber. *Sci. Rep. 7*, 6179.
- (9) Trent, J. T., Hvitved, A., and Hargrove, M. S. (2001) A model for ligand binding to hexacoordinate hemoglobins. *Biochemistry* 40, 6155–6163.
- (10) Simonneaux, G., and Bondon, A. (2005) Mechanism of electron transfer in heme proteins and models: the NMR approach. *Chem. Rev.* 105, 2627–2646.
- (11) Kiger, L., Tilleman, L., Geuens, E., Hoogewijs, D., Lechauve, C., Moens, L., Dewilde, S., and Marden, M. C. (2011) Electron transfer

function versus oxygen delivery: A comparative study for several hexacoordinated globins across the animal kingdom. *PLoS One 6*, e20478.

- (12) De Henau, S., Tilleman, L., Vangheel, M., Luyckx, E., Trashin, S., Pauwels, M., Germani, F., Vlaeminck, C., Vanfleteren, J. R., Bert, W., Pesce, A., Nardini, M., Bolognesi, M., De Wael, K., Moens, L., Dewilde, S., and Braeckman, B. P. (2015) A redox signalling globin is essential for reproduction in Caenorhabditis elegans. *Nat. Commun.* 6, 8782
- (13) He, B. Y., Schulz, C. E., and Li, J. F. (2015) Synthesis and characterization of a modified "picket fence" porphyrin complex stronger π bonding interactions between Fe(II) and axial ligands. *Dalton Trans.* 44, 13651–13661.
- (14) Marques, H. M. (2007) Insights into porphyrin chemistry provided by the microperoxidases, the haempeptides derived from cytochrome c. Dalton Trans. 0, 4371–4385.
- (15) Du, J., Perera, R., and Dawson, J. H. (2011) Alkylamine-ligated H93G myoglobin cavity mutant: a model system for endogenous lysine and terminal amine ligation in heme proteins such as nitrite reductase and cytochrome *f. Inorg. Chem. 50*, 1242–1249.
- (16) Reedy, C. J., and Gibney, B. R. (2004) Heme protein assemblies. *Chem. Rev.* 104, 617–649.
- (17) Lu, Y., Berry, S. M., and Pfister, T. D. (2001) Engineering novel metalloproteins: Design of metal-binding sites into native protein scaffolds. *Chem. Rev.* 101, 3047–3080.
- (18) Yu, F., Cangelosi, V. M., Zastrow, M. L., Tegoni, M., Plegaria, J. S., Tebo, A. G., Mocny, C. S., Ruckthong, L., Qayyum, H., and Pecoraro, V. L. (2014) Protein Design: Toward Functional Metalloenzymes. *Chem. Rev.* 114, 3495–3578.
- (19) Nastri, F., Chino, M., Maglio, O., Bhagi-Damodaran, A., Lu, Y., and Lombardi, A. (2016) Design and engineering of artificial oxygenactivating metalloenzymes. *Chem. Soc. Rev.* 45, 5020–5054.
- (20) Farid, T. A., Kodali, G., Solomon, L. A., Lichtenstein, B. R., Sheehan, M. M., Fry, B. A., Bialas, C., Ennist, N. M., Siedlecki, J. A., Zhao, Z., Stetz, M. A., Valentine, K. G., Anderson, J. L. R., Wand, A. J., Discher, B. M., Moser, C. C., and Dutton, P. L. (2013) Elementary tetrahelical protein design for diverse oxidoreductase functions. *Nat. Chem. Biol.* 9, 826–833.
- (21) Makino, M., Sawai, H., Shiro, Y., and Sugimoto, H. (2011) Crystal structure of the carbon monoxide complex of human cytoglobin. *Proteins: Struct., Funct., Genet.* 79, 1143–1153.
- (22) Vallone, B., Nienhaus, K., Matthes, A., Brunori, M., and Nienhaus, G. U. (2004) The structure of carbonmonoxy neuroglobin reveals a heme-sliding mechanism for control of ligand affinity. *Proc. Natl. Acad. Sci. U. S. A.* 101, 17351–17356.
- (23) de Sanctis, D., Ascenzi, P., Bocedi, A., Dewilde, S., Burmester, T., Hankeln, T., Moens, L., and Bolognesi, M. (2006) Cyanide binding and heme cavity conformational transitions in *Drosophila melanogaster* hexacoordinate hemoglobin. *Biochemistry* 45, 10054–10061.
- (24) Rosell, F. I., Ferrer, J. C., and Mauk, A. G. (1998) Proton-linked protein conformational switching: Definition of the alkaline conformational transition of yeast iso-1-ferricytochrome c. J. Am. Chem. Soc. 120, 11234–11245.
- (25) Ferrer, J. C., Guillemette, J. G., Bogumil, R., Inglis, S. C., Smith, M., and Mauk, A. G. (1993) Identification of Lys79 as an iron ligand in one form of alkaline yeast iso-1-ferricytochrome *c. J. Am. Chem. Soc.* 115, 7507—7508.
- (26) Pearce, L. L., Gartner, A. L., Smith, M., and Mauk, A. G. (1989) Mutation-induced perturbation of the cytochrome *c* alkaline transition. *Biochemistry* 28, 3152–3156.
- (27) Josephs, T. M., Liptak, M. D., Hughes, G., Lo, A., Smith, R. M., Wilbanks, S. M., Bren, K. L., and Ledgerwood, E. C. (2013) Conformational change and human cytochrome *c* function: mutation of residue 41 modulates caspase activation and destabilizes Met-80 coordination. *JBIC, J. Biol. Inorg. Chem.* 18, 289–297.
- (28) Nall, B. T., Zuniga, E. H., White, T. B., Wood, L. C., and Ramdas, L. (1989) Replacement of a conserved proline and the alkaline conformational change in iso-2-cytochrome c. Biochemistry 28, 9834–9839.

(29) Goldes, M. E., Jeakins-Cooley, M. E., McClelland, L. J., Mou, T. C., and Bowler, B. E. (2016) Disruption of a hydrogen bond network in human versus spider monkey cytochrome *c* affects heme crevice stability. *J. Inorg. Biochem.* 158, 62–69.

- (30) Wenke, B. B., Lecomte, J. T. J., Heroux, A., and Schlessman, J. L. (2014) The 2/2 hemoglobin from the cyanobacterium *Synechococcus* sp. PCC 7002 with covalently attached heme: comparison of X-ray and NMR structures. *Proteins: Struct., Funct., Genet.* 82, 528–534.
- (31) Scott, N. L., Falzone, C. J., Vuletich, D. A., Zhao, J., Bryant, D. A., and Lecomte, J. T. J. (2002) The hemoglobin of the cyanobacterium *Synechococcus* sp. PCC 7002: Evidence for hexacoordination and covalent adduct formation in the ferric recombinant protein. *Biochemistry* 41, 6902–6910.
- (32) Nothnagel, H. J., Preimesberger, M. R., Pond, M. P., Winer, B. Y., Adney, E. M., and Lecomte, J. T. J. (2011) Chemical reactivity of *Synechococcus* sp. PCC 7002 and *Synechocystis* sp. PCC 6803 hemoglobins: covalent heme attachment and bishistidine coordination. *JBIC, J. Biol. Inorg. Chem.* 16, 539–552.
- (33) Preimesberger, M. R., Pond, M. P., Majumdar, A., and Lecomte, J. T. J. (2012) Electron self-exchange and self-amplified posttranslational modification in the hemoglobins from *Synechocystis* sp. PCC 6803 and *Synechococcus* sp. PCC 7002. *JBIC*, *J. Biol. Inorg. Chem.* 17, 599–609.
- (34) Vuletich, D. A., Falzone, C. J., and Lecomte, J. T. J. (2006) Structural and dynamic repercussions of heme binding and hemeprotein cross-linking in *Synechococcus* sp. PCC 7002 hemoglobin. *Biochemistry* 45, 14075–14084.
- (35) Pond, M. P., Majumdar, A., and Lecomte, J. T. J. (2012) Influence of heme post-translational modification and distal ligation on the backbone dynamics of a monomeric hemoglobin. *Biochemistry 51*, 5733–5747.
- (36) Rice, S. L., Preimesberger, M. R., Johnson, E. A., and Lecomte, J. T. J. (2014) Introduction of a covalent histidine-heme linkage in a hemoglobin: A promising tool for heme protein engineering. *J. Inorg. Biochem.* 141, 198–207.
- (37) Scott, N. L., and Lecomte, J. T. J. (2000) Cloning, expression, purification, and preliminary characterization of a putative hemoglobin from the cyanobacterium *Synechocystis* sp. PCC 6803. *Protein Sci.* 9, 587–597.
- (38) Teale, F. W. J. (1959) Cleavage of heme-protein link by acid methylethylketone. *Biochim. Biophys. Acta* 35, 543.
- (39) Neya, S., Nagai, M., Nagatomo, S., Hoshino, T., Yoneda, T., and Kawaguchi, A. T. (2016) Utility of heme analogues to intentionally modify heme-globin interactions in myoglobin. *Biochim. Biophys. Acta, Bioenerg.* 1857, 582–588.
- (40) Hendler, R. W., and Shrager, R. I. (1994) Deconvolutions based on singular value decomposition and the pseudoinverse: a guide for beginners. *J. Biochem. Biophys. Methods* 28, 1–33.
- (41) Wishart, D. S., Bigam, C. G., Yao, J., Abildgaard, F., Dyson, H. J., Oldfield, E., Markley, J. L., and Sykes, B. D. (1995) ¹H, ¹³C and ¹⁵N chemical shift referencing in biomolecular NMR. *J. Biomol. NMR* 6, 135–140.
- (42) Jeener, J., Meier, B. H., Bachmann, P., and Ernst, R. R. (1979) Investigation of exchange processes by two-dimensional NMR spectroscopy. *J. Chem. Phys.* 71, 4546–4553.
- (43) Farrow, N. A., Zhang, O., Forman-Kay, J. D., and Kay, L. E. (1994) A heteronuclear correlation experiment for simultaneous determination of ¹⁵N longitudinal decay and chemical exchange rates of systems in slow equilibrium. *J. Biomol. NMR* 4, 727–734.
- (44) Delory, G. E., and King, E. J. (1945) A sodium carbonate-bicarbonate buffer for alkaline phosphatases. *Biochem. J.* 39, 245.
- (45) Otting, G., Liepinsh, E., and Wüthrich, K. (1993) Disulfide bond isomerization in BPTI and BPTI(G36S): an NMR study of correlated mobility in proteins. *Biochemistry* 32, 3571–3582.
- (46) Hardman, C. H., Broadhurst, R. W., Raine, A. R. C., Grasser, K. D., Thomas, J. O., and Laue, E. D. (1995) Structure of the A-domain of HMG1 and its interaction with DNA as studied by heteronuclear three- and four-dimensional NMR spectroscopy. *Biochemistry* 34, 16596–16607.

(47) Pond, M. P., Vuletich, D. A., Falzone, C. J., Majumdar, A., and Lecomte, J. T. J. (2009) ¹H, ¹⁵N, and ¹³C resonance assignments of the 2/2 hemoglobin from the cyanobacterium *Synechococcus* sp. PCC 7002 in the ferric bis-histidine state. *Biomol. NMR Assignments* 3, 211–214.

- (48) Scott, N. L., Xu, Y., Shen, G., Vuletich, D. A., Falzone, C. J., Li, Z., Ludwig, M., Pond, M. P., Preimesberger, M. R., Bryant, D. A., and Lecomte, J. T. J. (2010) Functional and structural characterization of the 2/2 hemoglobin from *Synechococcus* sp. PCC 7002. *Biochemistry* 49, 7000–7011.
- (49) Preimesberger, M. R., Johnson, E. A., Nye, D. B., and Lecomte, J. T. J. (2017) Covalent attachment of the heme to *Synechococcus* hemoglobin alters its reactivity toward nitric oxide. *J. Inorg. Biochem.* 177, 171–182.
- (50) Pesce, A., Couture, M., Dewilde, S., Guertin, M., Yamauchi, K., Ascenzi, P., Moens, L., and Bolognesi, M. (2000) A novel two-overtwo α -helical sandwich fold is characteristic of the truncated hemoglobin family. *EMBO J.* 19, 2424–2434.
- (51) Banci, L., Bertini, I., Branchini, B. R., Hajieva, P., Spyroulias, G. A., and Turano, P. (2001) Dimethyl propionate ester heme-containing cytochrome b_5 : structure and stability. *JBIC, J. Biol. Inorg. Chem.* 6, 490–503.
- (52) Antonini, E., and Brunori, M. (1970) Hemoglobin. *Annu. Rev. Biochem.* 39, 977–1042.
- (53) Preimesberger, M. R., Majumdar, A., and Lecomte, J. T. J. (2017) The dynamics of lysine as a heme axial ligand: NMR analysis of the *Chlamydomonas reinhardtii* hemoglobin THB1. *Biochemistry* 56, 551–569.
- (54) Ubbink, M., Campos, A. P., Teixeira, M., Hunt, N. I., Hill, H. A., and Canters, G. W. (1994) Characterization of mutant Met100Lys of cytochrome *c*-550 from *Thiobacillus versutus* with lysine-histidine heme ligation. *Biochemistry* 33, 10051–10059.
- (55) Davis, L. A., Schejter, A., and Hess, G. P. (1974) Alkaline isomerization of oxidized cytochrome c. Equilibrium and kinetic measurements. J. Biol. Chem. 249, 2624–2632.
- (56) Tsuda, M., Shirotani, I., Minomura, S., and Terayama, Y. (1976) Effect of pressure on dissociation of weak acids in aqueous buffers. *Bull. Chem. Soc. Jpn.* 49, 2952–2955.
- (57) Markley, J. (1975) Observation of histidine residues in proteins by means of nuclear magnetic resonance spectroscopy. *Acc. Chem. Res.* 8, 70–80.
- (58) Preimesberger, M. R., Majumdar, A., Rice, S. L., Que, L., and Lecomte, J. T. J. (2015) Helix-capping histidines: Diversity of N-H···N hydrogen bond strength revealed by $^{2h}J_{\rm NN}$ scalar couplings. *Biochemistry* 54, 6896–6908.
- (59) Kroll, T., Hadt, R. G., Wilson, S. A., Lundberg, M., Yan, J. J., Weng, T. C., Sokaras, D., Alonso-Mori, R., Casa, D., Upton, M. H., Hedman, B., Hodgson, K. O., and Solomon, E. I. (2014) Resonant inelastic X-ray scattering on ferrous and ferric bis-imidazole porphyrin and cytochrome *c*: Nature and role of the axial methionine-Fe bond. *J. Am. Chem. Soc.* 136, 18087—18099.
- (60) Marques, H. M., Munro, O. Q., Munro, T., de Wet, M., and Vashi, P. R. (1999) Coordination of N-donor ligands by the monomeric ferric porphyrin N-acetylmicroperoxidase-8. *Inorg. Chem.* 38, 2312–2319.
- (61) Vallee, B. L., and Williams, R. J. (1968) Metalloenzymes: the entatic nature of their active sites. *Proc. Natl. Acad. Sci. U. S. A.* 59, 498–505.
- (62) Cowley, A. B., Kennedy, M. L., Silchenko, S., Lukat-Rodgers, G. S., Rodgers, K. R., and Benson, D. R. (2006) Insight into heme protein redox potential control and functional aspects of six-coordinate ligand-sensing heme proteins from studies of synthetic heme peptides. *Inorg. Chem.* 45, 9985–10001.
- (63) Das, D. K., and Medhi, O. K. (1998) The role of heme propionate in controlling the redox potential of heme: Square wave voltammetry of protoporphyrinato IX iron(III) in aqueous surfactant micelles. *J. Inorg. Biochem.* 70, 83–90.
- (64) Tonge, P., Moore, G. R., and Wharton, C. W. (1989) Fourier-transform infra-red studies of the alkaline isomerization of

mitochondrial cytochrome *c* and the ionization of carboxylic-acids. *Biochem. J.* 258, 599–605.

- (65) Hartshorn, R. T., and Moore, G. R. (1989) A denaturation-induced proton-uptake study of horse ferricytochrome *c. Biochem. J.* 258, 595–598.
- (66) Gu, J., Shin, D.-W., and Pletneva, E. V. (2017) Remote perturbations in tertiary contacts trigger ligation of lysine to the heme iron in cytochrome *c. Biochemistry* 56, 2950–2966.
- (67) Kakar, S., Hoffman, F. G., Storz, J. F., Fabian, M., and Hargrove, M. S. (2010) Structure and reactivity of hexacoordinate hemoglobins. *Biophys. Chem.* 152, 1–14.
- (68) Schneider, S., Marles-Wright, J., Sharp, K. H., and Paoli, M. (2007) Diversity and conservation of interactions for binding heme in b-type heme proteins. *Nat. Prod. Rep.* 24, 621–630.
- (69) Nienhaus, K., Kriegl, J. M., and Nienhaus, G. U. (2004) Structural dynamics in the active site of murine neuroglobin and its effects on ligand binding. *J. Biol. Chem.* 279, 22944–22952.
- (70) Kumar, N., Astegno, A., Chen, J., Giorgetti, A., and Dominici, P. (2016) Residues in the distal heme pocket of Arabidopsis non-symbiotic hemoglobins: Implication for nitrite reductase activity. *Int. J. Mol. Sci.* 17, 640.
- (71) Martínková, M., Kitanishi, K., and Shimizu, T. (2013) Hemebased globin-coupled oxygen sensors: Linking oxygen binding to functional regulation of diguanylate cyclase, histidine kinase, and methyl-accepting chemotaxis. *J. Biol. Chem.* 288, 27702–27711.
- (72) Gilles-Gonzalez, M. A., and Gonzalez, G. (2005) Heme-based sensors: defining characteristics, recent developments, and regulatory hypotheses. *J. Inorg. Biochem.* 99, 1–22.
- (73) Kurokawa, H., Lee, D. S., Watanabe, M., Sagami, I., Mikami, B., Raman, C. S., and Shimizu, T. (2004) A redox-controlled molecular switch revealed by the crystal structure of a bacterial heme PAS sensor. *J. Biol. Chem.* 279, 20186–20193.
- (74) Lanzilotta, W. N., Schuller, D. J., Thorsteinsson, M. V., Kerby, R. L., Roberts, G. P., and Poulos, T. L. (2000) Structure of the CO sensing transcription activator CooA. *Nat. Struct. Biol.* 7, 876–880.
- (75) Sun, Y. H., Zeng, W. Q., Benabbas, A., Ye, X., Denisov, I., Sligar, S. G., Du, J., Dawson, J. H., and Champion, P. M. (2013) Investigations of heme Ligation and ligand switching in cytochromes P450 and P420. *Biochemistry* 52, 5941–5951.
- (76) McClelland, L. J., Mou, T. C., Jeakins-Cooley, M. E., Sprang, S. R., and Bowler, B. E. (2014) Structure of a mitochondrial cytochrome *c* conformer competent for peroxidase activity. *Proc. Natl. Acad. Sci. U. S. A. 111*, 6648–6653.
- (77) Kagan, V. E., Tyurin, V. A., Jiang, J. F., Tyurina, Y. Y., Ritov, V. B., Amoscato, A. A., Osipov, A. N., Belikova, N. A., Kapralov, A. A., Kini, V., Vlasova, II, Zhao, Q., Zou, M. M., Di, P., Svistunenko, D. A., Kurnikov, I. V., and Borisenko, G. G. (2005) Cytochrome *c* acts as a cardiolipin oxygenase required for release of proapoptotic factors. *Nat. Chem. Biol.* 1, 223–232.
- (78) Bren, K. L., and Raven, E. L. (2017) Locked and loaded for apoptosis. *Science* 356, 1236–1236.
- (79) Mara, M. W., Hadt, R. G., Reinhard, M. E., Kroll, T., Lim, H., Hartsock, R. W., Alonso-Mori, R., Chollet, M., Glownia, J. M., Nelson, S., Sokaras, D., Kunnus, K., Hodgson, K. O., Hedman, B., Bergmann, U., Gaffney, K. J., and Solomon, E. I. (2017) Metalloprotein entatic control of ligand-metal bonds quantified by ultrafast x-ray spectroscopy. *Science* 356, 1276–1280.
- (80) Amacher, J. F., Zhong, F., Lisi, G. P., Zhu, M. Q., Alden, S. L., Hoke, K. R., Madden, D. R., and Pletneva, E. V. (2015) A compact structure of cytochrome *c* trapped in a lysine-ligated state: loop refolding and functional implications of a conformational switch. *J. Am. Chem. Soc.* 137, 8435–8449.
- (81) Yin, V., Shaw, G. S., and Konermann, L. (2017) Cytochrome c as a peroxidase: Activation of the pre-catalytic native state by H_2O_2 -induced covalent modifications. *J. Am. Chem. Soc.* 139, 15701–15709.
- (82) Barker, P. D., and Mauk, A. G. (1992) pH-Linked conformational regulation of a metalloprotein oxidation-reduction equilibrium: electrochemical analysis of the alkaline form of cytochrome *c. J. Am. Chem. Soc. 114*, 3619–3624.

(83) Nelson, C. J., and Bowler, B. E. (2000) pH dependence of formation of a partially unfolded state of a Lys 73 -> His variant of iso1-cytochrome *c*: Implications for the alkaline conformational transition of cytochrome *c*. *Biochemistry* 39, 13584–13594.

- (84) Fetrow, J. S., and Baxter, S. M. (1999) Assignment of ¹⁵N chemical shifts and ¹⁵N relaxation measurements for oxidized and reduced iso-1-cytochrome *c. Biochemistry 38*, 4480–4492.
- (85) Barker, P. D., Bertini, I., Del Conte, R., Ferguson, S. J., Hajieva, P., Tomlinson, E., Turano, P., and Viezzoli, M. S. (2001) A further clue to understanding the mobility of mitochondrial yeast cytochrome c: a 15 N $T_{1\rho}$ investigation of the oxidized and reduced species. *Eur. J. Biochem.* 268, 4468–4476.
- (86) Assfalg, M., Bertini, I., Turano, P., Mauk, A. G., Winkler, J. R., and Gray, H. B. (2003) ¹⁵N-¹H Residual dipolar coupling analysis of native and alkaline-K79A *Saccharomyces cerevisiae* cytochrome *c. Biophys. J. 84*, 3917–3923.
- (87) Sakamoto, K., Kamiya, M., Uchida, T., Kawano, K., and Ishimori, K. (2010) Redox-controlled backbone dynamics of human cytochrome *c* revealed by ¹⁵N NMR relaxation measurements. *Biochem. Biophys. Res. Commun.* 398, 231–236.
- (88) Imai, M., Saio, T., Kumeta, H., Uchida, T., Inagaki, F., and Ishimori, K. (2016) Investigation of the redox-dependent modulation of structure and dynamics in human cytochrome c. Biochem. Biophys. Res. Commun. 469, 978–984.
- (89) Ying, T., Zhong, F., Xie, J., Feng, Y., Wang, Z. H., Huang, Z. X., and Tan, X. (2009) Evolutionary alkaline transition in human cytochrome c. J. Bioenerg. Biomembr. 41, 251–257.
- (90) Andrew, C. R., Petrova, O. N., Lamarre, I., Lambry, J.-C., Rappaport, F., and Negrerie, M. (2016) The dynamics behind the affinity: Controlling heme-gas affinity via geminate recombination and heme propionate conformation in the NO carrier cytochrome c'. ACS Chem. Biol. 11, 3191–3201.
- (91) Bhagi-Damodaran, A., Petrik, I. D., Marshall, N. M., Robinson, H., and Lu, Y. (2014) Systematic tuning of heme redox potentials and its effects on O_2 reduction rates in a designed oxidase in myoglobin. *J. Am. Chem. Soc.* 136, 11882–11885.
- (92) Brändén, G., Brändén, M., Schmidt, B., Mills, D. A., Ferguson-Miller, S., and Brzezinski, P. (2005) The protonation state of a heme propionate controls electron transfer in cytochrome *c* oxidase. *Biochemistry* 44, 10466–10474.
- (93) Warren, J. J., and Mayer, J. M. (2011) Proton-coupled electron transfer reactions at a heme-propionate in an iron-protoporphyrin-IX model compound. *J. Am. Chem. Soc.* 133, 8544–8551.
- (94) Mauk, M. R., Mauk, A. G., Weber, P. C., and Matthew, J. B. (1986) Electrostatic analysis of the interaction of cytochrome c with native and dimethyl ester heme substituted cytochrome b_5 . Biochemistry 25, 7085–7091.